

Periodic electron oscillation in coupled two-dimensional lattices

Yan-Yan Lu(陆艳艳), Chao Wang(王超), Jin-Yi Jiang(将金益), Jie Liu(刘洁), and Jian-Xin Zhong(钟建新)
Citation: Chin. Phys. B, 2023, 32 (**7**): 070306. DOI: 10.1088/1674-1056/acce93
Journal homepage: http://cpb.iphy.ac.cn; http://iopscience.iop.org/cpb

What follows is a list of articles you may be interested in

Engineering topological state transfer in four-period Su-Schrieffer-Heeger chain

Xi-Xi Bao(包茜茜), Gang-Feng Guo(郭刚峰), and Lei Tan(谭磊)
Chin. Phys. B, 2023, 32 (**2**): 020301. DOI: 10.1088/1674-1056/ac7bfe

Probability density and oscillating period of magnetopolaron in parabolic quantum dot in the presence of Rashba effect and temperature

Ying-Jie Chen(陈英杰) and Feng-Lan Shao(邵凤兰)
Chin. Phys. B, 2021, 30 (**11**): 110304. DOI: 10.1088/1674-1056/abfa0b

Quantum to classical transition induced by a classically small influence

Wen-Lei Zhao(赵文垒), Quanlin Jie(揭泉林)
Chin. Phys. B, 2020, 29 (**8**): 080302. DOI: 10.1088/1674-1056/ab8a3a

microtoroidal resonator coupled systems

Cao Cong (曹聪), Liu Gang (刘刚), Zhang Ru (张茹), Wang Chuan (王川)
Chin. Phys. B, 2014, 23 (**4**): 040304. DOI: 10.1088/1674-1056/23/4/040304

Nonlinear resonance phenomenon of one-dimensional Bose–Einstein condensate under periodic modulation

Hua Wei (花巍), Liu Shi-Xing (刘世兴)
Chin. Phys. B, 2014, 23 (**2**): 020309. DOI: 10.1088/1674-1056/23/2/020309

RAPID COMMUNICATION

Periodic electron oscillation in coupled two-dimensional lattices

Yan-Yan Lu(陆艳艳), Chao Wang(王超), Jin-Yi Jiang(将金益), Jie Liu(刘洁), and Jian-Xin Zhong(钟建新)[†]

Hunan Key Laboratory of Micro-Nano Energy Materials and Devices, School of Physics and Optoelectronics, Xiangtan University, Hunan 411105, *China*

(Received 27 March 2023; revised manuscript received 18 April 2023; accepted manuscript online 20 April 2023)

We study the time evolution of electron wavepacket in the coupled two-dimensional (2D) lattices with mirror symmetry, utilizing the tight-binding Hamiltonian framework. We show analytically that the wavepacket of an electron initially located on one atomic layer in the coupled 2D square lattices exhibits a periodic oscillation in both the transverse and longitudinal directions. The frequency of this oscillation is determined by the strength of the interlayer hopping. Additionally, we provide numerical evidence that a damped periodic oscillation occurs in the coupled 2D disordered lattices with degree of disorder W, with the decay time being inversely proportional to the square of W and the frequency change being proportional to the square of W, which is similar to the case in the coupled 1D disordered lattices. Our numerical results further confirm that the periodic and damped periodic electron oscillations are universal, independent of lattice geometry, as demonstrated in AA-stacked bilayer and tri-layer graphene systems. Unlike the Bloch oscillation driven by electric fields, the periodic oscillation induced by interlayer coupling does not require the application of an electric field, has an ultrafast periodicity much shorter than the electron decoherence time in real materials, and can be tuned by adjusting the interlayer coupling. Our findings pave the way for future observation of periodic electron oscillation in material systems at the atomic scale.

Keywords: quantum diffusion, periodic oscillation, coupled systems, disorder, Anderson localization

PACS: 03.65.–w, 71.23.–k, 72.10.–d, 72.80.Ng **DOI:** 10.1088/1674-1056/acce93

1. Introduction

The Bloch oscillation is a quantum phenomenon that occurs in periodic lattices due to Bragg reflection when electrons are subjected to a constant electric field, which differs significantly from the behavior of accelerated motion in classical physics.[1,2] It is further proved[3,4] that a constant electronic field transforms the continuous electronic band spectrum of a periodic lattice into a series of equidistant energy levels separated by the energy spacing $\Delta E = eFa$ and superposition of the localized Wannie–Stark eigen-states results in periodic oscillation of electrons with temporal periodicity $T_{\rm B} = h/(eFa)$ and spatial width $L_{\rm B} = W_{\rm B}/(eF)$, where $W_{\rm B}$, F, a, e and h are the electronic bandwidth, the applied electronic field, the lattice spacing, the electron charge, and the Planck constant, respectively. It was very difficult to realize the Bloch oscillation in crystals due to the bearing capacity of electronic field in real materials and the lose of electron coherence caused by impurities, defects, and atomic thermal vibrations. Two approaches have been employed to observe the Bloch quantum oscillation in periodic systems, focusing on either increasing the lattice spacing or increasing the coherence time. After 60 years of its prediction, Bloch oscillation was first observed successfully in semiconductor superlattices by significantly enlarged the superlattice spacing in the order of thousands of times larger than the atomic scale.[5–7] In recent years, systems of cold atoms in optical potential lattices have been widely used to simulate and study quantum behaviors of electrons in solids because of longer decoherence time for atoms and wide range of tunability for lattice geometry and lattice spacing as well as atom–potential and atom–atom interactions. The Bloch oscillation of cold atoms has been realized in various experimental setups.[8–14] The Bloch oscillation of quantum particles in periodic systems in nature is a phenomenon of wave scattering and thus has also been observed in optical[15–19] and phonon systems[20] in recent years. Nevertheless, it has been a great challenge to realize periodic electron oscillation in materials at atomic scale.

We recently found that quantum diffusion of electrons (time evolution of electron wavepackets) in the coupled two identical one-dimensional (1D) lattices of mirror symmetry exhibits a well-defined periodic oscillation with a frequency determined by the interchain hopping strength and undergoes a damped periodic oscillation when random perturbation of site potentials exists.[21] In this paper, using coupled square lattices as a model system, we expand upon the theory of periodic electron oscillation for coupled 1D lattices to coupled 2D crystals of multiple atomic layers with mirror symmetry in the framework of tight-binding Hamiltonian. We show that the wavepacket of an electron initially located on one atomic layer in the coupled 2D lattices exhibits the same type of periodic oscillation or damped periodic oscillation (with disordered potentials) in both transverse and longitudinal directions with the frequency determined by the interlayer hopping strength. With the research advances in 2D materials

[†]Corresponding author. E-mail: jxzhong@xtu.edu.cn

© 2023 Chinese Physical Society and IOP Publishing Ltd

in recent years, few-layer graphene can be routinely obtained experimentally.[22–28] We numerically study quantum diffusion in the AA-stacked bilayer and tri-layer graphene films with mirror symmetry to verify the universality of the periodic oscillation independent of lattice geometry and to provide theoretical guidance for its possible experimental realization.

2. Theory

On the basis of the periodic oscillation of quantum diffusion in the coupled two identical 1D lattices of mirror symmetry,[21] we develop a general theory for periodic electron oscillation in the coupled multiple layers of identical 2D lattices of mirror symmetry. The system of coupled square lattices of m layers shown in Fig. 1 with lattice spacing a and lattice sites N for each layer is used to present the theory. The Hamiltonian of the system H has the following tight-binding form:

$$H = \sum_{\alpha=1}^{m} H^{\alpha} + \sum_{\alpha,\beta}^{m} H^{\alpha,\beta}, \tag{1}$$

where H^{α} is the sub-Hamiltonian for each layer and $H^{\alpha,\beta}$ represents the coupling between different layers. In the framework of tight-bonding scheme with nearest-neighbor hopping, H^{α} and $H^{\alpha,\beta}$ are given by

$$H^{\alpha} = \sum_{i=1}^{N} \varepsilon_i^{\alpha} |\alpha,i\rangle\langle\alpha,i| + \sum_{i,j}^{N} V_{i,j}^{\alpha} |\alpha,i\rangle\langle\alpha,j|, \tag{2}$$

$$H^{\alpha,\beta} = \sum_{i}^{m} V_{i,i}^{\alpha,\beta} |\alpha,i\rangle\langle\beta,i|, \tag{3}$$

where $|\alpha,i\rangle$ is the local atomic orbital at site i of α layer, ε_i^{α} is the corresponding onsite energy, $V_{i,j}^{\alpha}$ and $V_{i,i}^{\alpha,\beta}$ are the nearest-neighboring intralayer and interlayer hopping parameters, respectively. For the coupled system of identical layers of mirror symmetry, uniform distribution of hopping energy is considered with two parameters to represent the intralayer and interlayer hopping strengths, namely, $V_{i,j}^{\alpha} = v$ and $V_{i,i}^{\alpha,\beta} = u$.

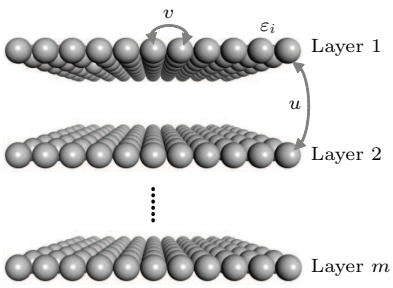


Fig. 1. Schematic illustration of the system for coupled 2D atomic layers of square lattice with mirror symmetry. Parameters ε_i, v, and u correspond to onsite potential, nearest-neighboring intralayer hoping and interlayer hoping, respectively.

The eigen-states of the coupled lattices are given by the Schrödinger equation $\boldsymbol{H}|\psi\rangle = E|\psi\rangle$, where E and $|\psi\rangle$ are the eigenenergy and eigenvector, respectively, which can be derived from the iso-spectrum e_l $(l = 1,2,\ldots,N)$ and their corresponding eigenvector $|\phi_l^{\alpha}\rangle$ for the m identical layers given by Schrödinger equations $\boldsymbol{H}^{\alpha}|V_l^{\alpha}\rangle = e_l|V_l^{\alpha}\rangle$ with

$$|\phi_l^{\alpha}\rangle = \sum_{i=1}^{N} \boldsymbol{U}_{l,i} |\alpha,i\rangle, \tag{4}$$

where $\boldsymbol{U}_{l,i} = \langle\alpha,i|\phi_l^{\alpha}\rangle$ is a unitary matrix. In the basis set $|\phi_l^{\alpha}\rangle$, one has

$$\boldsymbol{H}_{l,l'}^{\alpha} = \langle\phi_l^{\alpha}|\boldsymbol{H}^{\alpha}|\phi_{l'}^{\alpha}\rangle = e_l\delta_{l,l'}, \tag{5}$$

$$\boldsymbol{H}_{l,l'}^{\alpha,\beta} = \langle\phi_l^{\alpha}|\boldsymbol{H}^{\alpha,\beta}|\phi_{l'}^{\beta}\rangle = u\delta_{l,l'}. \tag{6}$$

The Hamiltonian matrix $\boldsymbol{H}$ is thus block diagonal in the basis of $|\phi_l^{\alpha}\rangle$ for different eigenstates with the following $m \times m$ block matrix:

$$\boldsymbol{H}_l = \begin{bmatrix} e_l & u & 0 & 0 & \cdots & 0 \\ u & e_l & u & 0 & \cdots & 0 \\ 0 & u & e_l & \ddots & \ddots & \vdots \\ 0 & 0 & \ddots & \ddots & u & 0 \\ \vdots & \vdots & \ddots & u & e_l & u \\ 0 & 0 & \cdots & 0 & u & e_l \end{bmatrix}. \tag{7}$$

Eigenenergy E and eigenvector $|\psi\rangle$ of the coupled system of m identical 2D layers can be obtained from Eq. (7).

For the system of coupled two 2D lattices, eigenenergy E_k $(k = 1,2,\ldots,2N)$ and eigenvector $|\psi_k\rangle$ are given by two sets of values $E_l^{\pm}$ and their corresponding eigenvectors $|\psi_l^{\pm}\rangle$ from Eq. (7)

$$E_l^{\pm} = e_l \pm u, \tag{8a}$$

$$|\psi_l^{\pm}\rangle = \frac{1}{\sqrt{2}}\left(|\phi_l^1\rangle \pm |\phi_l^2\rangle\right). \tag{8b}$$

For the system of coupled three 2D lattices, eigenenergy E_k $(k = 1,2,\ldots,3N)$ and eigenvector $|\psi_k\rangle$ are given by the three sets of values E_l^0, E_l^+ and E_l^- and their corresponding eigenvectors from Eq. (7)

$$E_l^0 = e_l, \quad E_l^{\pm} = e_l \pm \sqrt{2}u, \tag{9a}$$

$$|\psi_l^0\rangle = \frac{1}{\sqrt{2}}\left(|\phi_l^1\rangle - |\phi_l^3\rangle\right),$$

$$|\psi_l^{\pm}\rangle = \frac{1}{2}\left(|\phi_l^1\rangle \pm \sqrt{2}|\phi_l^2\rangle + |\phi_l^3\rangle\right). \tag{9b}$$

The time evolution of an electron wave packet[29,30] in the coupled layers is described in general by

$$\Psi(t) = \sum_{k=1}^{m\times N} C_k |\psi_k\rangle \, \mathrm{e}^{-\mathrm{i}E_k t}, \tag{10}$$

where coefficient C_k is determined by the initial condition of the wave packet. We note that t in Eq. (10) is rescaled by the Planck constant $\hbar$. Assuming the electron is initially located at site n_0 on layer 1, one has $C_k = \langle\psi_k/1,n_0\rangle$. Substituting Eqs. (8) and (9) into Eq. (10), we can derive the analytical form of $\Psi(t)$ for the coupled two layers and three layers.

For the system of coupled two 2D lattices,

$$\Psi(t) = \sum_{l=1}^{N} \frac{1}{2} U_{l,n_0}^{*} \, \mathrm{e}^{-\mathrm{i}e_l t}\left[\left(|\phi_l^1\rangle + |\phi_l^2\rangle\right) \mathrm{e}^{-\mathrm{i}ut}\right.$$

$$+\left(\left|\phi_l^1\right\rangle-\left|\phi_l^2\right\rangle\right)\mathrm{e}^{\mathrm{i}ut}\Big]. \tag{11}$$

Projecting $\Psi(t)$ to local orbitals of lattice sites, we have the wavefunction at site n on different layers $\Psi_n^{(\alpha)}(t)$ with

$$\Psi_n^{(1)}(t)=\langle 1,n|\Psi(t)\rangle=\cos(ut)\,B_n(t), \tag{12a}$$
$$\Psi_n^{(2)}(t)=\langle 2,n|\Psi(t)\rangle=\sin(ut)\,B_n(t), \tag{12b}$$

where $B_n(t)=\sum_{l=1}^{N}U_{l,n}U_{l,n_0}^{*}\,\mathrm{e}^{-\mathrm{i}e_l t}$ is the wavefunction at site n for the isolated layer without interlayer coupling. The probability of finding electron at site n follows

$$P_n^{(1)}(t)=\cos^2(ut)\,B_n^2(t), \tag{13a}$$
$$P_n^{(2)}(t)=\sin^2(ut)\,B_n^2(t). \tag{13b}$$

The probability of finding electron on different layers is thus given by

$$P_1(t)=\cos^2(ut), \tag{14a}$$
$$P_2(t)=\sin^2(ut). \tag{14b}$$

The spreading width of wavepacket $d(t)$ in the coupled lattices is described by $d(t)=\sqrt{d_1^2(t)+d_2^2(t)}$, where $d_1(t)$ and $d_2(t)$ are spreading widths on different layers with

$$d_1^2(t)=\sum_{n=1}^{N}P_n^{(1)}(t)\Delta^2\boldsymbol{r}_n, \tag{15a}$$
$$d_2^2(t)=\sum_{n=1}^{N}P_n^{(2)}(t)(a^2+\Delta^2\boldsymbol{r}_n), \tag{15b}$$

where $\Delta\boldsymbol{r}_n=\boldsymbol{r}_n-\boldsymbol{r}_{n_0}$ is the planar position difference. Substitution of Eq. (13) into Eq. (15) leads to

$$d_1^2(t)=P_1(t)d_{\mathrm{s}}^2(t), \tag{16a}$$
$$d_2^2(t)=P_2(t)\left[a^2+d_{\mathrm{s}}^2(t)\right], \tag{16b}$$

with $d_{\mathrm{s}}^2(t)=\sum_{n=1}^{N}B_n^2(t)\,\Delta^2\boldsymbol{r}_n$, where $d_{\mathrm{s}}(t)$ is the spreading width of the wavepacket on the isolated single layer without coupling.

For the system of coupled three layers of 2D square lattices with electron initially located at a site on the top layer, we have

$$\Psi(t)=\sum_{l=1}^{N}\frac{1}{2}U_{l,n_0}^{*}\Big[\left|\psi_l^{+}\right\rangle\mathrm{e}^{-\mathrm{i}E_l^{+}t}+\sqrt{2}\left|\psi_l^{0}\right\rangle\mathrm{e}^{-\mathrm{i}E_l^{0}t}+\left|\psi_l^{-}\right\rangle\mathrm{e}^{-\mathrm{i}E_l^{-}t}\Big]. \tag{17}$$

From Eq. (9) and projecting $\Psi(t)$ to local orbitals of lattice sites, we have the wavefunction $\Psi_n^{(\alpha)}(t)$ at site n on different layers

$$\Psi_n^{(1)}(t)=\langle 1,n|\Psi(t)\rangle=\frac{1}{2}[\cos(\sqrt{2}ut)+1]B_n(t), \tag{18a}$$
$$\Psi_n^{(2)}(t)=\langle 2,n|\Psi(t)\rangle=-\frac{1}{\sqrt{2}}\sin\left(\sqrt{2}ut\right)B_n(t), \tag{18b}$$
$$\Psi_n^{(1)}(t)=\langle 3,n|\Psi(t)\rangle=\frac{1}{2}[\cos(\sqrt{2}ut)-1]B_n(t). \tag{18c}$$

The probability of finding electron on different layers is thus given by

$$P_1(t)=\frac{1}{4}\left[\cos\left(\sqrt{2}ut\right)+1\right]^2, \tag{19a}$$
$$P_2(t)=\frac{1}{2}\sin^2\left(\sqrt{2}ut\right), \tag{19b}$$
$$P_3(t)=\frac{1}{4}\left[\cos\left(\sqrt{2}ut\right)-1\right]^2. \tag{19c}$$

The spreading widths on different layers follow

$$d_1^2(t)=P_1(t)d_{\mathrm{s}}^2(t), \tag{20a}$$
$$d_2^2(t)=P_2(t)\left[a^2+d_{\mathrm{s}}^2(t)\right], \tag{20b}$$
$$d_1^2(t)=P_3(t)\left[4a^2+d_{\mathrm{s}}^2(t)\right], \tag{20c}$$

where $d_{\mathrm{s}}(t)$ is the spreading width of the wavepacket on the isolated single layer without coupling. The form of periodic oscillation depends on the initial position of the electron. When the electron is initially located at a site on the middle layer, we have

$$P_1(t)=P_3(t)=\frac{1}{2}\sin^2\left(\sqrt{2}ut\right), \tag{21a}$$
$$P_2(t)=\cos^2\left(\sqrt{2}ut\right) \tag{21b}$$

and

$$d_1^2(t)=d_3^2(t)=P_1(t)\left[a^2+d_{\mathrm{s}}^2(t)\right], \tag{22a}$$
$$d_2^2(t)=P_2(t)d_{\mathrm{s}}^2(t). \tag{22b}$$

For large time, since $d_{\mathrm{s}}(t)\approx d(t)$ due to $d_{\mathrm{s}}(t)\gg a$, Eqs. (16), (20), and (22) indicate that the fluctuation of spreading width on different layers is given by $\bar{d}_\alpha^2(t)=d_\alpha^2(t)/d^2(t)=P_\alpha(t)$. Therefore, the probability of finding electron and the spreading width on each layer exhibit a well-defined periodic oscillation with frequencies determined by the interlayer hopping strength. For the system of coupled two layers with electron initially located on one layer, the oscillation frequency is $f_0=u/\pi$. For the coupled system of three layers with electron initially located on the middle layer, electron appears on different layers with an oscillation frequency $f_0=\sqrt{2}u/\pi$. For the coupled system of three layers with electron initially located on the outer layer, the occurrence oscillation frequencies for middle layer and outer layers are $f_0=\sqrt{2}u/\pi$ and $f_1=u/\sqrt{2}\pi$, respectively. From the above theoretical analysis, one can see that the existence of the periodic oscillation is a result of energy level splitting of the iso-spectrum for the identical 2D crystals under interlayer coupling, independent of the system size and boundary condition. Therefore, the periodic oscillation persistently exists before and after the wavepacket reaches the boundary. Equations (8a) and (9a) indicate that the level of energy splitting is of the order of interlayer hopping strength u. Thus, one expects that the periodic oscillation

exists in the coupled disordered 2D crystals if the strength of disorder is smaller than u. This is indeed the case in the coupled identical 1D systems with Anderson disorder of strength W, where a damped periodic oscillation occurs with a decay time inversely proportional to the square of W and a slight frequency change proportional to the square of W.[21] It is interesting to examine if the behavior of damped periodic oscillation still holds in the coupled 2D lattices.

3. Numerical results

We use the coupled two/three identical layers of square lattice to numerically illustrate the periodic electron oscillation. The system size of $N = 51 \times 51 \times 2$ and open boundary condition are used in the calculations. The method of direct diagonalization of Hamiltonian is employed to directly solve the static and time-dependent Schrödinger equations and calculate the wavefunctions, probabilities of finding electron, spreading widths of electronic wavepackets. The initial location of the electron is at the center of layer 1.

Figure 2 illustrates the behavior of quantum diffusion in the coupled bilayers with $\varepsilon_i = 0$, $v = 1$, and $u = 1$. Figure 2(a) shows that the spreading width of wavepacket $d(t)$ increases linearly with time and stops increasing after the wavepacket reaches the boundary at $t \approx 10.5$ as shown by the probability of finding electron $P_{\rm b}(t)$ on boundary sites in the upper inset of Fig. 2(a). Further analysis of the numerical results confirms that $P_\alpha(t)$ ($\alpha = 1,2$) and the fluctuation part of $d_\alpha(t)$ exhibit the periodic oscillation at any time (before or after the wavepacket reaches the boundary) with the frequency of $f_0 = u/\pi$ given by Eqs. (14) and (16). As examples, behaviors of periodic oscillation of $P_\alpha(t)$ and $d_\alpha(t)$ are illustrated in the lower insects in Fig. 2(a) for time intervals $0 \le t \le 10.5$ and $75 \le t \le 85$ corresponding to the cases for the wavepacket before reaching and after reaching the boundary, respectively. Examples of onsite distributions of probability $P_n^{(1)}(t)$ and $P_n^{(2)}(t)$ on different layers at the time after different successive periods of oscillation are shown in Fig. 2(b). One can clearly see that the wavepacket occurs only on the upper layer at $t = 3.14$ or the bottom layer at $t = 4.71$ and repeats the same behavior at $t = 590.62$ or $t = 592.19$, spreading out on two layers alternatively with the periodicity given by $f_0 = u/\pi$.

Disorder may exist in the system of coupled layers. We use the Anderson-type model of disorder.[21,31–34] to examine the stability of the periodic oscillation against disorder by adding a random value in the interval $[-W,W]$ to all onsite energies of the system. Through analysis of $P_\alpha(t)$ and $d_\alpha(t)$ on the system of disordered coupled bilayers, we find that $P_\alpha(t)$ and $\bar{d}_\alpha^2(t)$ exhibit the same damped periodic oscillation as found in coupled 1D systems described by

$$P_\alpha(t) = \bar{d}_\alpha^2(t) = \frac{1}{2} \pm \frac{1}{2} \mathrm{e}^{-t/t_0} \cos(2ft), \tag{23}$$

where the decay time t_0 follows $t_0 \sim W^{-2}$ and the frequency parameter f has a slight increase as W increases described by $\Delta f = f - f_0 \sim W^2$.

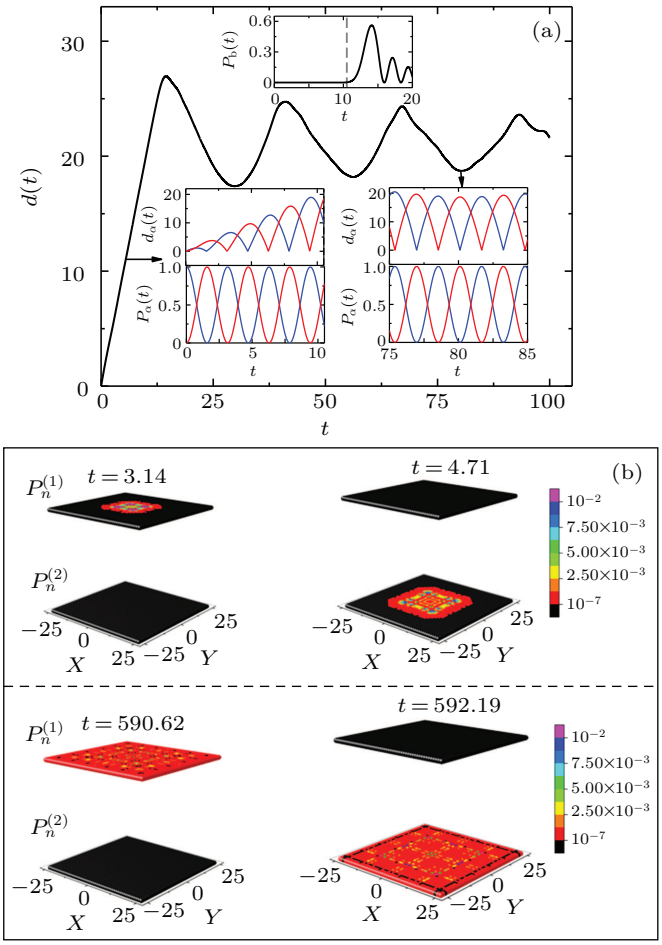


Fig. 2. Time evolution of wave packet in the coupled bilayer square lattices with $N = 51 \times 51 \times 2$, $\varepsilon_i = 0$, $v = 1$, and $u = 1$. (a) Spreading width of the wave packet $d(t)$ in the coupled system and associated spreading width $d_\alpha(t)$ and probability $P_\alpha(t)$ on layer 1 (blue line) and layer 2 (red line) in two typical time intervals as marked by arrows. The upper inset shows the total probability of finding electron $P_{\rm b}(t)$ at boundary sites and the time of the wave packet reaching the boundary is marked by dashed line. (b) Onsite distributions of wave packet $P_n^{(1)}(t)$ on layer 1 and $P_n^{(2)}(t)$ on layer 2 at the time after 1 ($t = 3.14$), 1.5 ($t = 4.71$) periods of oscillation and 188 ($t = 590.62$), 188.5 ($t = 592.19$) periods of oscillation.

Figure 3 illustrates quantum diffusion in disordered bilayers of size $N = 51 \times 51 \times 2$ with 20 different configurations of disorder, where $v = 1$, $u = 1$, and $\varepsilon_i \in [-W,W]$. Figure 3(a) shows the behavior of $d(t)$ with $W = 1$. As expected, $d(t)$ stops increase before reaching the boundary as shown in Fig. 3(a) due to the localization of eigenstates in the 2D disordered systems. The oscillation length $d_\alpha(t)$ and probability $P_\alpha(t)$ still show periodic oscillation, but their amplitudes decay with time. As examples, the periodic oscillations of $d_\alpha(t)$ and probability $P_\alpha(t)$ are shown in the insets of Fig. 3(a) during time intervals $0 \le t \le 25$. We focus on the analysis of $P_1(t)$ and $d_1(t)$ due to $P_1(t) + P_2(t) = 1$ and $d_1^2(t) + d_2^2(t) = d^2(t)$. Figure 3(b) shows the FFT frequency spectra of $P_1(t)$ during time intervals $0 \le t \le 500$ for different

values of W. From Fig. 3(b), one can see that the spectrum has only one frequency peak under small W in all cases, locating at almost the same position for $W = 0$. Under large disorder, the frequency distribution widens significantly, indicating the absence of periodic oscillation of single frequency. Probability $P_1(t)$ and spreading width $\bar{d}_1^2(t)$ for different values of W and their fit to Eq. (23) are shown in Figs. 3(c) and 3(d), in which parameter t_0 is from the linear fit of the plot of $\ln(2P_1 - 1)$ against t as shown in Fig. 3(e), where P_1 is the peak value of $P_1(t)$. Parameter f is from fitting numerical results of $P_1(t)$ and $\bar{d}_1^2(t)$ to Eq. (23). Values of t_0 and f versus W in Fig. 3(f) clearly show that the data can be well fitted by $t_0 \sim W^{-2}$ and $\Delta f = f - f_0 \sim W^2$.

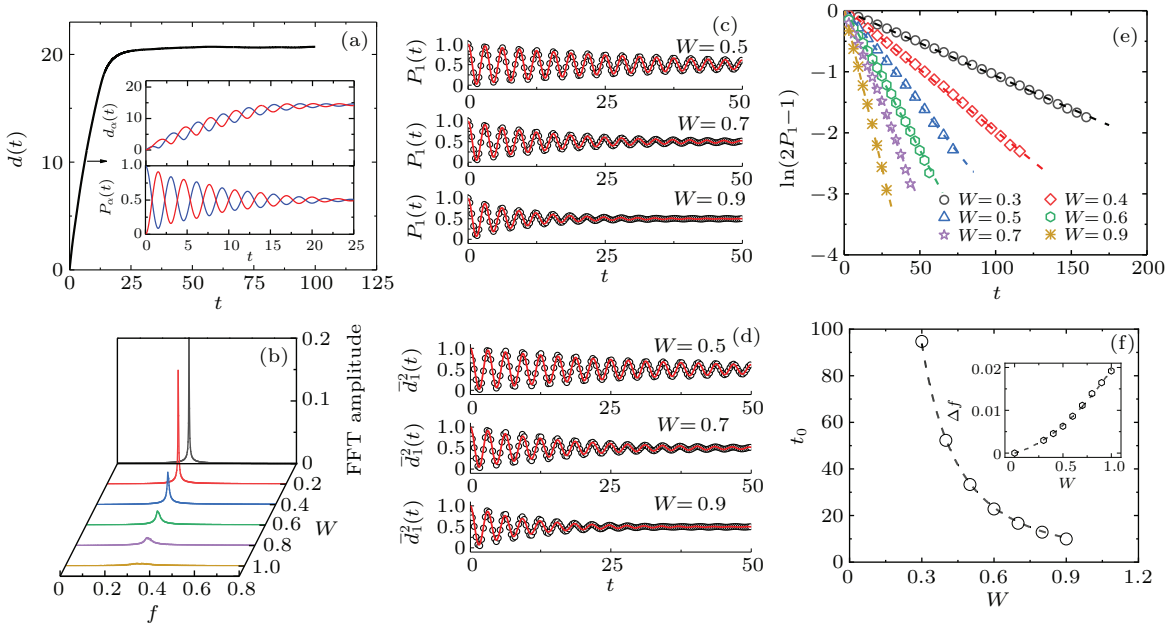


Fig. 3. Time evolution of wave packet in the coupled disordered 2D square lattices with $N = 51 \times 51 \times 2$, $v = 1$, $u = 1$, $\varepsilon_i \in [-W, W]$ and different degrees of disorder W. (a) Spreading width of wave packet $d(t)$ with $W = 1$ and associated spreading width $d_\alpha(t)$ and probability $P_\alpha(t)$ on layer 1 (blue line) and layer 2 (red line) in the time intervals as marked by arrow. (b) FFT frequency spectrum of probability $P_1(t)$ as a function of W. (c) and (d) $P_1(t)$ and $\bar{d}_1^2(t) = d_1^2(t)/d^2(t)$ for $W = 0.5, 0.7, 0.9$ (open circles) and corresponding fitting results (lines) with $t_0 = 33.3, 16.6, 9.9$ and $f = 1.006, 1.011, 1.016$, respectively. (e) $\ln(2P_1 - 1)$ versus t for $W = 0.3, 0.4, 0.5, 0.6, 0.7, 0.9$ (symbols) and corresponding linear fitting results (lines) with $t_0 = 94.7, 52.3, 33.3, 22.8, 16.6, 9.9$, respectively, where P_1 is the peak value of $P_1(t)$. (f) Values of t_0 and f versus W (symbols) and corresponding fitting results (lines) to $t_0 \sim W^{-2}$ and $\Delta f = f - f_0 \sim W^2$ (inset).

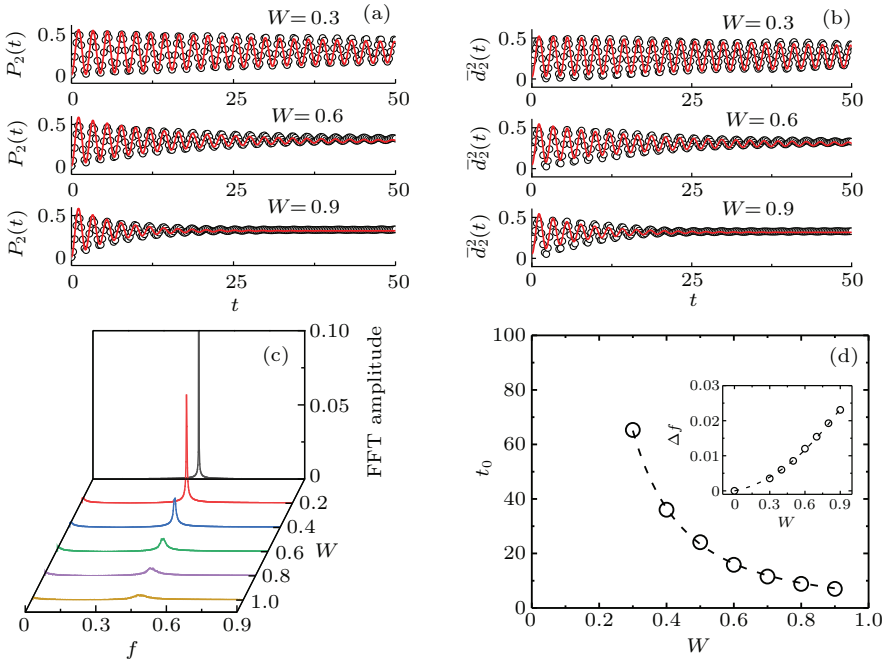


Fig. 4. Time evolution of wave packet in the coupled disordered 2D square lattices of three layers with $N = 51 \times 51 \times 3$, $v = 1$, $u = 1$, $\varepsilon_i \in [-W, W]$ and different degrees of disorder W. (a) and (b) $P_2(t)$ and $\bar{d}_2^2(t) = d_2^2(t)/d^2(t)$ for $W = 0.3$, 0.6, 0.9 (open circles) and corresponding fitting results (lines) with $t_0 = 65.28$, 15.83, 6.98 and $f = 1.41774$, 1.42621, 1.43728, respectively. (c) FFT frequency spectrum of probability $P_2(t)$ as a function of W. (d) Values of t_0 and f versus W (symbols) and corresponding fitting results (lines) to $t_0 \sim W^{-2}$ and $\Delta f = f - f_0 \sim W^2$.

For the coupled system of three layers, we focus on analysis of $P_2(t)$ and $\bar{d}_2^2(t)$ since $P_1(t)$ and $\bar{d}_1^2(t)$ display the same behavior of $P_3(t)$ and $\bar{d}_3^2(t)$ which is given by $P_1(t)+P_2(t)+P_3(t)=1$, and $\bar{d}_1^2(t)+\bar{d}_2^2(t)+\bar{d}_3^2(t)=1$. The size of the system for numerical calculation is $N=51\times51\times3$ with the same Hamiltonian parameters as used for the coupled bilayers. Our numerical results for the coupled three periodic 2D lattices agree well with the analytical results described in Eqs. (19)–(22). Moreover, the electron exhibits the same type of damped periodic oscillation under disordered perturbation as shown in Figs. 4(a) and 4(b) for $P_2(t)$ and $\bar{d}_2^2(t)$, respectively. And the numerical results are from the average of 20 different disordered configurations. Figure 4(c) gives the FFT frequency spectra of $P_2(t)$ for different values of W, which shows that the spectrum has only one frequency peak under small W in all cases, locating at almost the same position for $W=0$ given by $f_0=\sqrt{2}u/\pi$. For large disorder, the frequency distribution widens significantly, indicating the absence of periodic oscillation of single frequency. Through the same fitting process, we find that $P_2(t)$ and $\bar{d}_2^2(t)$ for different values of W are described by

$$P_2(t)=\bar{d}_2^2(t)=c_1+c_1\,\mathrm{e}^{-t/t_0}\cos(2ft). \tag{24}$$

The perfect fit of the damped periodic oscillation to Eq. (24) can be seen in Figs. 4(a) and 4(b). The relationship between the values of t_0 and W is described by $t_0\sim W^{-2}$ shown in Fig. 4(d). The slight change of frequency can be well fitted by $\Delta f=f-f_0\sim W^2$ as shown in inset of Fig. 4(d).

4. Coupled system of graphene layers

We apply the theory to AA-stacked bilayer and tri-layer graphene films with mirror symmetry for verifying the universality of periodic oscillation as well as for the possible experimental realization of periodic electron oscillation. The system size used is $N=7688$ with $x=31\times2a$, $y=31\times\frac{\sqrt{3}}{2}a$, $z=d$, where a is lattice spacing equal to 0.142 nm, and d is the distance between the layers equal to 0.335 nm, nearest-neighbor intralayer hoping $v=-2.7$ eV.[35,36] In the case of disordered bilayer graphene, numerical results are from the average of 20 different disordered configurations for reliable results.

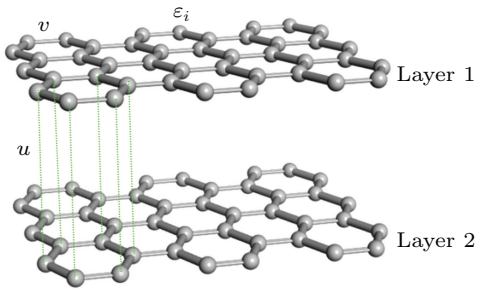


Fig. 5. Schematic illustration of coupled bilayer graphene layers with mirror symmetry (AA stacking). Parameters ε_i, v, and u correspond to onsite potential, nearest-neighboring intralayer hoping, and interlayer hoping, respectively.

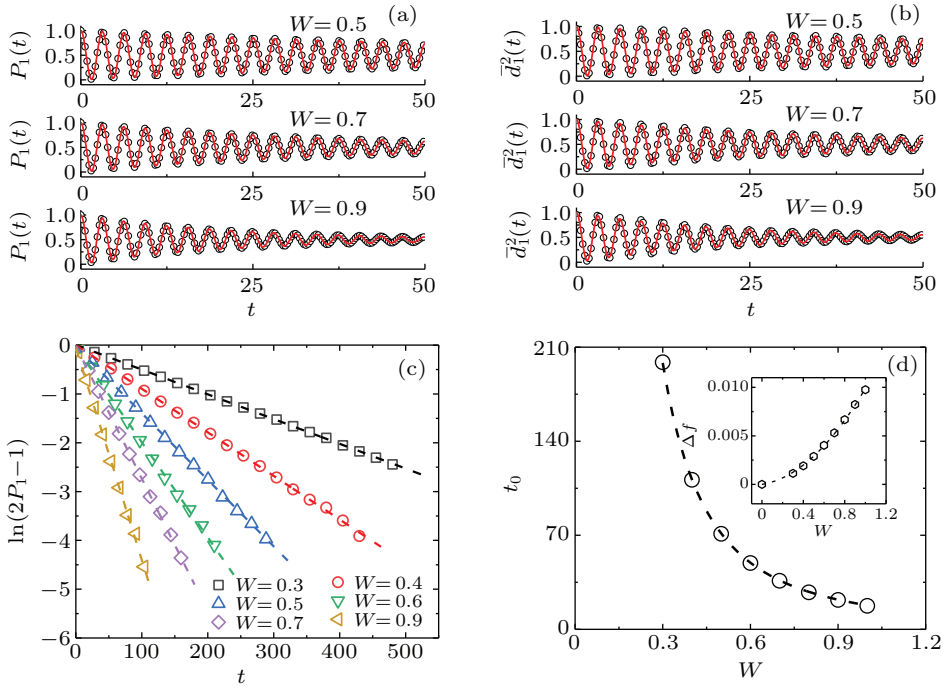


Fig. 6. Time evolution of wave packet in the coupled bilayer graphene with $N=3844\times2$, $v=2.7$, $u=1$, $\varepsilon_i\in[-W,W]$ and different degrees of disorder W. (a) and (b) $P_1(t)$ and $\bar{d}_1^2(t)$ for $W=0.5$, 0.7, 0.9 (open circles) and corresponding fitting results (lines) with $t_0=71.115$, 36.112, 21.858 and $f=1.00288$, 1.00531, 1.00823, respectively. (c) The plot of the values of $\ln(2P_1-1)$ versus t for $W=0.3$, 0.4, 0.5, 0.6, 0.7, 0.9 (symbols) and corresponding linear fitting results (lines) with $t_0=198.78$, 111.3, 71.115, 49.328, 36.111, 21.858, respectively, and P_1 is the peak value of $P_1(t)$. (d) Values of t_0 and f versus W (symbols) and corresponding fitting results (lines) to $t_0\sim W^{-2}$ and $\Delta f=f-f_0\sim W^2$ (inset).

Electron in bilayer graphene exhibits the same periodic oscillation with the frequency given by $f_0=u/\pi$ and the same behavior of damped periodic oscillation described in Eq. (23). Figures 6(a) and 6(b) illustrate the damped periodic oscillations of

$P_1(t)$ and $\bar{d}_1^2(t)$, respectively. From the amplitudes of the damped oscillation, we obtain the characteristic decay time t_0 through fitting as shown in Fig. 6(c). By substituting t_0 into Eq. (23) and fitting the data of $P_1(t)$ and $\bar{d}_1^2(t)$ to Eq. (23), we obtain the frequency f of the damped periodic oscillation. Excellent fits to $P_1(t)$ and $\bar{d}_1^2(t)$ can be seen from Figs. 6(a) and 6(b). Changes of t_0 and f with W are shown in Fig. 6(d). The relationship between the values of t_0 and W is described by $t_0 \sim W^{-2}$. Inset of Fig. 6(d) shows that $\Delta f = f - f_0 \sim W^2$.

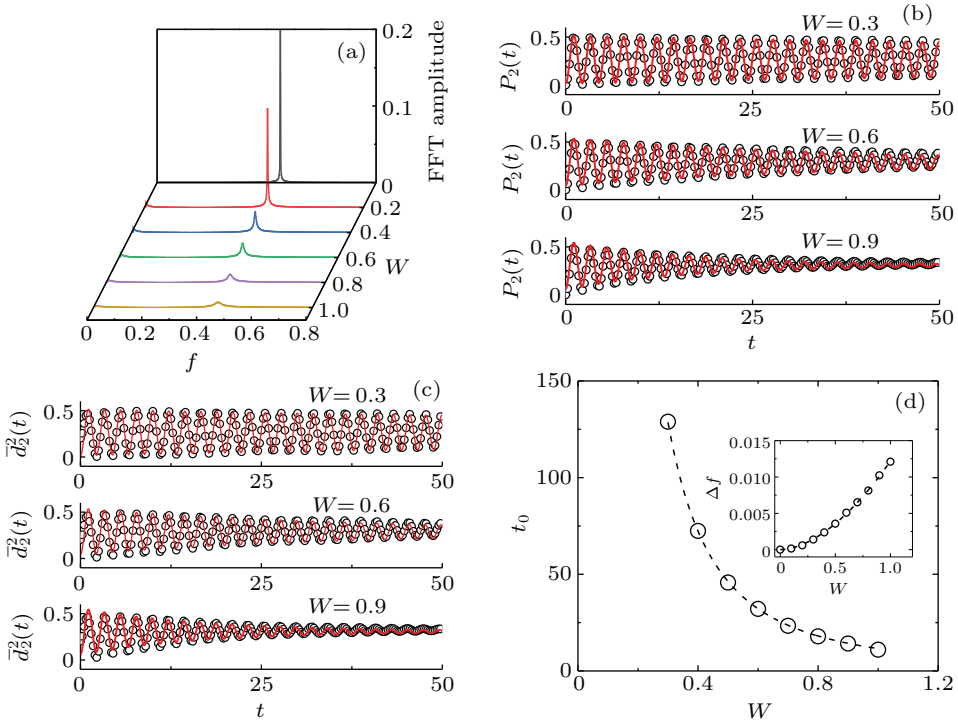


Fig. 7. Time evolution of wave packet in the coupled tri-layer graphene with $N = 3844 \times 3$, $v = 2.7$, $u = 1$, $\varepsilon_i \in [-W, W]$ and different degrees of disorder W. (a) FFT frequency spectrum of probability $P_2(t)$ as a function of W. (b) and (c) $P_2(t)$ and $\bar{d}_2^2(t)$ for $W = 0.3$, 0.6, 0.9 (open circles) and corresponding fitting results (lines) with $t_0 = 128.88$, 32.096, 14.16 and $f = 1.41561$, 1.4193, 1.42443, respectively. (d) Values of t_0 and f versus W (symbols) and corresponding fitting results (lines) to $t_0 \sim W^{-2}$ and $\Delta f = f - f_0 \sim W^2$.

For the tri-layer graphene, electron displays the same periodic oscillation behavior as in bilayer graphene but with different frequencies $f_0 = \sqrt{2}u/\pi$, and $f_1 = u/\sqrt{2}\pi$ given by Eqs. (19)–(22). When disorder exists, the damped periodic oscillation is described by Eq. (24). Figure 7(a) illustrates the frequency distribution of damped oscillations of $P_2(t)$ as W increases, which shows a distinctive peak around the intrinsic frequency under weak disorder $W < u$. Figures 7(b) and 7(c) illustrate the calculation results and their excellent fits to the damped periodic oscillation described by Eq. (24). Again, one finds $t_0 \sim W^{-2}$ and $\Delta f = f - f_0 \sim W^2$ as shown in Fig. 7(d).

5. Discussion and conclusions

In summary, we have developed a general theory for the periodic oscillation of electronic wavepacket spreading in coupled systems of 2D periodic crystals with mirror symmetry in the framework of tight-binding Hamiltonian without disorder or with disordered potentials. Using coupled bilayer and tri-layer 2D square lattices, we analytically and numerically showed that time evolution of an electronic wavepacket initially distributed on one atomic layer exhibits a periodic oscillation in both vertical direction and horizontal direction with frequencies determined by the interlayer hopping strength and the number of atomic layers. The underlying mechanism for the periodic oscillation is the equal-level splitting of every level of the iso-spectrum of the identical 2D lattices, irrelevant to the system size and boundary condition. We further examined the stability of the periodic oscillation in coupled 2D crystals with disordered site potentials and numerically show that the wavepacket undergoes the same behavior of damped periodic oscillation as found in the coupled 1D disordered systems. Finally, we applied the theory to the AA-stacked bilayer and tri-layer graphene of honeycomb lattice with mirror symmetry and found the same behaviors of periodic oscillation and damped periodic oscillation, which provide a theoretical guidance for the observation of the periodic oscillation in experiments. The periodic oscillation here for the coupled systems of 2D crystals with mirror symmetry has the same forms found in the coupled 1D systems with mirror symmetry.[21] This universal periodic oscillation can be understood from the physical perspective of the mirror symmetry of the Hamiltonian and the effect of finite size quantum confinement. Under transverse mirror symmetry, the electron wavefunction in

the coupled identical 2D systems (or 1D systems) is given by the product of the 2D system (or 1D system) and the wavefunction of the transverse chain of finite size composed of m atoms ($m \geq 2$).[29] The confinement of electron under finite size along transverse direction results in the periodic oscillation of electron within the distance of m atoms, which in turn leads to the periodic oscillation along the longitudinal direction within the spreading width of the wavepacket determined by the 2D (or 1D) system. Because the periodic oscillation is caused by the transverse chain of m atoms of mirror symmetry, its frequency is determined solely by the interlayer (or interchain) coupling strength, irrelevant to the dimensionality and the type of onsite potentials in the 2D (or 1D) systems. It is intriguing that the disorder results in the same behavior of damped periodic oscillation both in coupled 1D systems and 2D crystals with the universal scaling behaviors $t_0 \sim W^{-2}$ and $\Delta f = f - f_0 \sim W^2$, which might come from the similarity of localization of wavefunctions in 1D and 2D disordered electron systems.

The periodic electron oscillation in coupled 2D crystals shares some common features with Bloch oscillation driven by electronic field. In both cases, the electron exhibits periodic oscillation at atomic scale with ultra-high frequencies. For the coupling-induced oscillation, the electron oscillates periodically between different layers and its width increases with time when the wavepacket does not reach the system boundary and is determined by the system lateral size for longer time. The spatial width of the Bloch oscillation is finite determined by the electric field. The periodicity of the Bloch oscillation is given by $T_{\rm B} = h/(eFa)$. Because the bearing capacity of electric filed in materials is in the range of $F \sim 10^5$–10^7 V/m, one has $T_{\rm B} \sim 10^{-10}$–10^{-12} s, which is larger than the electron decoherence time in materials. Considering the rescaling factor Planck constant $\hbar$, one has the realistic periodicity for the coupled bilayer system given by $T_{\rm C} = h/(2u)$. Because the interlayer coupling is in the rage of 0.01 eV to 1 eV, we have $T_{\rm C} \sim 10^{-13}$–10^{-15} s, which is much smaller than the electron decoherence time in crystals. The coupling induced periodic oscillation has unique advantages over Bloch oscillation, including no need of applying electric field, faster oscillation with the periodicity much shorter than the electron decoherence time, and tunability by adjusting the interlayer coupling strength. Our model for the coupled 2D atomic layers paves the way for future observation of periodic electron oscillation in material systems at the atomic scale.

Acknowledgements

Project supported by the National Natural Science Foundation of China (Grant No. 11874316), the National Basic Research Program of China (Grant No. 2015CB921103), and the International Visiting Faculty Program of Hunan Provincial Government, China.

References

[1] Bloch F 1928 *Z. Phys.* **52** 555
[2] Zener C 1934 *Proc. R. Soc. London A* **145** 523
[3] Wannier G H 1962 *Rev. Mod. Phys.* **34** 645
[4] Wannier G H 1960 *Phys. Rev.* **117** 432
[5] Waschke C, Roskos H G, Schwedler R, Leo K, Kurz H and Köhler K 1993 *Phys. Rev. Lett.* **70** 3319
[6] Leo K, Bolivar P H, Brüggemann F, Schwedler R and Köhler K 1992 *Solid State Commun.* **84** 943
[7] Feldmann J, Leo K, Shah J, Miller D A, Cunningham J, Meier T, Von Plessen G, Schulze A, Thomas P and Schmitt-Rink S 1992 *Phys. Rev. B* **46** 7252
[8] Roati G, De Mirandes E, Ferlaino F, Ott H, Modugno G and Inguscio M 2004 *Phys. Rev. Lett.* **92** 230402
[9] Morsch O, Müller J, Cristiani M, Ciampini D and Arimondo E 2001 *Phys. Rev. Lett.* **87** 140402
[10] Dahan M B, Peik E, Reichel J, Castin Y and Salomon C 1996 *Phys. Rev. Lett.* **76** 4508
[11] Battesti R, Cladé P, Guellati-Khélifa S, Schwob C, Grémaud B, Nez F, Julien L and Biraben F 2004 *Phys. Rev. Lett.* **92** 253001
[12] Gustavsson M, Haller E, Mark M, Danzl J G, Rojas-Kopeinig G and Nägerl H C 2008 *Phys. Rev. Lett.* **100** 080404
[13] Ferrari G, Poli N, Sorrentino F and Tino G 2006 *Phys. Rev. Lett.* **97** 060402
[14] Wilkinson S, Bharucha C, Madison K, Niu Q and Raizen M 1996 *Phys. Rev. Lett.* **76** 4512
[15] Lenz G, Talanina I and De Sterke C M 1999 *Phys. Rev. Lett.* **83** 963
[16] Dreisow F, Szameit A, Heinrich M, Pertsch T, Nolte S, Tünnermann A and Longhi S 2009 *Phys. Rev. Lett.* **102** 076802
[17] Morandotti R, Peschel U, Aitchison J, Eisenberg H and Silberberg Y 1999 *Phys. Rev. Lett.* **83** 4756
[18] Corrielli G, Crespi A, Della Valle G, Longhi S and Osellame R 2013 *Nat. Commun.* **4** 1555
[19] Pertsch T, Dannberg P, Elflein W, Bräuer A and Lederer F 1999 *Phys. Rev. Lett.* **83** 4752
[20] Gutiérrez L, Díaz-de-Anda A, Flores J, Méndez-Sánchez R, Monsivais G and Morales A 2006 *Phys. Rev. Lett.* **97** 114301
[21] Jiang J, Lu Y, Wang C, Mosseri R and Zhong J 2022 *Sci. China-Phys. Mech. Astron.* **65** 247211
[22] Zhang Y, Tang T T, Girit C, Hao Z, Martin M C, Zettl A, Crommie M F, Shen Y R and Wang F 2009 *Nature* **459** 820
[23] Novoselov K S, Geim A K, Morozov S V, Jiang D E, Zhang Y, Dubonos S V, Grigorieva I V and Firsov A A 2004 *Science* **306** 666
[24] Chen G, Sharpe A L, Gallagher P, Rosen I T, Fox E J, Jiang L, Lyu B, Li H, Watanabe K and Taniguchi T 2019 *Nature* **572** 215
[25] Liu Y W, Su Y, Zhou X F, Yin L J, Yan C, Li S Y, Yan W, Han S, Fu Z Q and Zhang Y 2020 *Phys. Rev. Lett.* **125** 236102
[26] Novoselov K S, McCann E, Morozov S, Fal'ko V I, Katsnelson M, Zeitler U, Jiang D, Schedin F and Geim A 2006 *Nat. Phys.* **2** 177
[27] Cao Y, Fatemi V, Fang S, Watanabe K, Taniguchi T, Kaxiras E and Jarillo-Herrero P 2018 *Nature* **556** 43
[28] McCann E and Fal'ko V I 2006 *Phys. Rev. Lett.* **96** 086805
[29] Zhong J and Mosseri R 1995 *J. Phys. Condens. Matter* **7** 8383
[30] Zhong J, Diener R, Steck D A, Oskay W H, Raizen M G, Plummer E W, Zhang Z and Niu Q 2001 *Phys. Rev. Lett.* **86** 2485
[31] Anderson P W 1958 *Phys. Rev.* **109** 1492
[32] Thouless D J 1974 *Phys. Rep.* **13** 93
[33] Mott N F 1968 *Rev. Mod. Phys.* **40** 677
[34] Abrahams E, Anderson P, Licciardello D and Ramakrishnan T 1979 *Phys. Rev. Lett.* **42** 673
[35] Koshino M and Son Y W 2019 *Phys. Rev. B* **100** 075416
[36] Moon P and Koshino M 2013 *Phys. Rev. B* **88** 241412